MOLECULAR AND CELLULAR BIOLOGY, Apr. 2009, p. 2168–2180 Vol. 29, No. 8
0270-7306/09/$08.00+0 doi:10.1128/MCB.01508-08

c-Jun N-Terminal Kinase 1 Phosphorylates Myt1 To Prevent UVA-Induced Skin Cancer▽

Hong Seok Choi,[2] Ann M. Bode,[1] Jung-Hyun Shim,[1] Sung-Young Lee,[1] and Zigang Dong[1]*

The Hormel Institute, University of Minnesota, Austin, Minnesota 55912,[1] and College of Pharmacy, Chosun University, Seosuk-dong, Dong-gu, Gwangju 501-759, South Korea[2]

Received 26 September 2008/Returned for modification 1 November 2008/Accepted 30 January 2009

The c-Jun N-terminal kinase (JNK) signaling pathway is known to mediate both survival and apoptosis of tumor cells. Although JNK1 and JNK2 have been shown to differentially regulate the development of skin cancer, the underlying mechanistic basis remains unclear. Here, we demonstrate that JNK1, but not JNK2, interacts with and phosphorylates Myt1 ex vivo and in vitro. UVA induces substantial apoptosis in *JNK* wild-type (*JNK*$^{+/+}$) or *JNK2*-deficient (*JNK2*$^{-/-}$) mouse embryonic fibroblasts but has no effect on JNK1-deficient (*JNK1*$^{-/-}$) cells. In addition, UVA-induced caspase-3 cleavage and DNA fragmentation were suppressed by the knockdown of human *Myt1* in skin cancer cells. *JNK1* deficiency results in suppressed Myt1 phosphorylation and caspase-3 cleavage in skin exposed to UVA irradiation. In contrast, the absence of *JNK2* induces Myt1 phosphorylation and caspase-3 cleavage in skin exposed to UVA. The overexpression of *JNK1* with *Myt1* promotes cellular apoptosis during the early embryonic development of *Xenopus laevis*, whereas the presence of *JNK2* reduces the phenotype of Myt1-induced apoptotic cell death. Most importantly, *JNK1*$^{-/-}$ mice developed more UVA-induced papillomas than either *JNK*$^{+/+}$ or *JNK2*$^{-/-}$ mice, which was associated with suppressed Myt1 phosphorylation and decreased caspase-3 cleavage. Taken together, these data provide mechanistic insights into the distinct roles of the different JNK isoforms, specifically suggesting that the JNK1-mediated phosphorylation of Myt1 plays an important role in UVA-induced apoptosis and the prevention of skin carcinogenesis.

The c-Jun N-terminal kinases (JNKs) are members of the mitogen-activated protein kinase family of proteins (47). Three genes encode the JNK protein kinases, and mice lacking each of these genes exhibit a different phenotype (8). The *JNK1* and *JNK2* genes are expressed ubiquitously, whereas the *JNK3* gene has a more limited pattern of expression and is largely restricted to the brain, heart, and testes (8). The JNK signaling transduction pathway is activated by numerous extracellular stimuli, leading to varied and seemingly contradictory cellular responses (2, 21). Indeed, the JNK pathway has been implicated in both apoptosis and survival signaling (20). Thus, the individual JNK isoforms very likely perform different signaling functions.

Several lines of evidence suggest that JNKs play an important role in tumor cells. Ras-induced transformation is known to require c-Jun (22), and Ras induces c-Jun phosphorylation on sites that are phosphorylated by JNKs (38, 41). In addition, JNKs have been shown to be constitutively activated in several tumor cell lines, and the transforming action of several oncogenes has been reported to be JNK dependent (20). On the other hand, the double knockout of *JNK1* and *JNK2* (*JNK1*$^{-/-}$/*JNK2*$^{-/-}$) in fibroblasts caused marked increases in the number and growth of Ras-induced tumor nodules in vivo (24). These studies indicated that a key fundamental question remains unresolved concerning the ability of cells to interpret JNK activation in distinctly different ways (e.g., oncokinase versus tumor suppressor). This ability may very likely be mediated by specific substrate choices for JNK1, JNK2, or JNK3 within cells, but distinct substrates are yet to be identified.

Skin tumor formation occurs in three stages: initiation, promotion, and progression (1). UV radiation can act as a complete carcinogen, operating at each of these stages (1). Chronic UVA radiation alone induces photoaging and leads to the formation of papillomas and squamous cell carcinoma in mouse models (9, 23, 43). On the other hand, a recent report indicated that UV induces apoptosis mediated through the JNK/cytochrome *c*/caspase-3 pathway (44). Furthermore, UVA irradiation was shown to strongly induce H2AX phosphorylation that was mediated by JNKs, and the phosphorylation of H2AX by JNKs was required for apoptosis to occur through the caspase-3/caspase-activated DNase pathway (26). These observations confirm that the JNK signaling pathway is required for the response to some, but not all, apoptotic stimuli. The opposing roles of JNKs have been attributed to the observation that JNKs activate different substrates based on specific stimulus, cell-type, or temporal aspects. Thus, finding a new substrate that directly interacts with specific JNKs for apoptotic signaling is extremely important.

Here, we report that UVA irradiation strongly induced Myt1 phosphorylation that was mediated by JNK1, but not JNK2, and that JNK1-mediated phosphorylation of Myt1 was associated with the induction of apoptosis in skin cancer cells. These data showed that Myt1, a novel substrate of JNK1, is required for apoptosis occurring through caspase-3 activation and leads to the suppression of UVA-induced skin cancer development.

MATERIALS AND METHODS

Reagents and antibodies. Chemical reagents, including DMBA [dimethylbenz(a)nthracene], Tris, NaCl, and sodium dodecyl sulfate (SDS), for molecular biology and buffer preparation were purchased from Sigma-Aldrich (St. Louis,

* Corresponding author. Mailing address: The Hormel Institute, University of Minnesota, 801 16th Avenue NE, Austin, MN 55912. Phone: (507) 437-9600. Fax: (507) 437-9606. E-mail: zgdong@hi.umn.edu.

▽ Published ahead of print on 9 February 2009.

MO). Restriction enzymes and some modifying enzymes were obtained from New England BioLabs, Inc. (Beverly, MA). Cell culture medium and other supplements were purchased from Invitrogen (Carlsbad, CA). The DNA ligation kit (version 2.0) was from Takara Bio, Inc. (Otsu, Shiga, Japan). [γ-^{32}P]ATP and [^{35}S]methionine were purchased from Amersham Biosciences (Piscataway, NJ). Antibodies for the immunoblotting analysis were purchased from Cell Signaling Technology, Inc. (Beverly, MA), Santa Cruz Biotechnology, Inc. (Santa Cruz, CA), or Upstate Biotechnology, Inc. (Charlottesville, VA). The Check-Mate mammalian two-hybrid system, including expression vectors and the reporter luciferase vector, was obtained from Promega Corp. (Madison, WI).

Cell culture conditions and transfection. Human embryonic kidney 293 (HEK293) and human malignant melanoma (SK-MEL-28) cells were purchased from the American Type Culture Collection (ATCC) and cultured in Dulbecco's modified Eagle's medium (DMEM) or minimum essential medium (MEM) supplemented with 10% fetal bovine serum (FBS). *JNK*$^{+/+}$, *JNK1*$^{-/-}$, and *JNK2*$^{-/-}$ mouse embryonic fibroblasts (MEFs) were cultured in DMEM supplemented with 10% FBS.

Construction of mammalian expression and small interfering RNA (siRNA) vectors. For the mammalian two-hybrid (M2-H) system, the cDNAs of 50 human kinases were amplified by PCR and each introduced into the pACT or pBIND two-hybrid system vector. In this system, pBIND and pACT (Promega) are fusion vectors used for the linkage of proteins to the GAL4 DNA binding domain and to the VP16 transactivation domain. pcDNA3.0/Flag-JNK1, -JNK2, and -JNK3 were generated by PCR and subcloned into the pcDNA3.1/V5-HisA vector (Invitrogen, Carlsbad, CA). The segment encoding the full coding sequence of the selected human kinase candidate, in this case JNK1 or JNK3, was amplified by PCR and cloned in frame into the BamHI/XbaI sites for the pBIND fusion vector to produce plasmids pBIND-JNK1 and pBIND-JNK3 and the JNK1 and JNK3 deletion mutants. The pCS3-myc-Myt1 wild type (WT), pCS3-myc-Myt1-ΔC91, pCS3-myc-Myt1-ΔN102, pCS3-myc-Myt1-ΔN102ΔC91, and pGEX-KG-Myt1 were a gift from Tony Hunter (The Salk Institute, CA). For the knockdown of human Myt1, a validated Stealth RNAi DuoPak of human Myt1 was purchased from Invitrogen (Carlsbad, CA) and was introduced following the recommended protocols using jetSI-ENDO (Polyplus-transfection, Inc., New York, NY).

In vitro binding assay and GST protein expression. For the expression of the V5 epitope-tagged JNK1, JNK2, and JNK3 and the JNK1 and JNK3 deletion mutants, the appropriate plasmids (pcDNA3.1/V5-JNK1, -JNK2, and -JNK3 and for deletion mutants JNK1 and JNK3) were translated in vitro with L-[^{35}S] methionine using the T_NT Quick coupled transcription/translation system (Promega). For the glutathione *S*-transferase (GST) pull-down assay, 5 μg GST fusion protein of Myt1 was collected on glutathione-Sepharose beads (Amersham Biosciences) and incubated for 4 h at 4°C with [^{35}S]-labeled JNK1, JNK2, or JNK3. The bound proteins were denatured in sample buffer and separated by 10 to 20% SDS-polyacrylamide gel electrophoresis (PAGE), and expression was detected by autoradiography (Kodak, New Haven, CT).

Mammalian two-hybrid assay. The DNAs, pACT-histone Myt1, pBIND-JNK1, pBIND-JNK3, and pG5-luciferase were combined in the same molar ratio and the total amount of DNA was not more than 100 ng/well. The transfection was performed using the Fugene 6 reagent as described by the manufacturer's recommended protocols. The cells were disrupted by the addition of 200 μl of cell lysis buffer directly into each well of the 48-well plate, and then aliquots of 100 μl were added to individual wells of a 96-well luminescence plate. The luminescence activity was measured automatically by a computer program (MTX Lab, Inc., Vienna, VA). The relative luciferase activity was calculated and normalized based on the pG5-luciferase basal control. For the assessment of the transfection efficiency and protein amount, the *Renilla* luciferase activity assay or the Lowry protein assay was used.

Immunoblotting and kinase assays. Cells were disrupted in lysis buffer (50 mM Tris [pH 7.5], 5 mM EDTA, 150 mM NaCl, 1 mM dithiothreitol, 0.01% Nonidet P-40, 0.2 mM phenylmethylsulfonyl fluoride, and 1× protease inhibitor cocktail). The proteins were resolved by sodium dodecyl (lauryl) sulfate-PAGE and transferred onto polyvinylidene fluoride membranes. The membranes were blocked and hybridized with the appropriate primary antibody overnight at 4°C. Protein bands were visualized with a chemiluminescence detection kit (ECL; Amersham Biosciences) after hybridization with the horseradish peroxidase-conjugated secondary antibody from a rabbit or mouse. Recombinant full-length human JNK1-, JNK2-, and JNK3-activated proteins were from Upstate.

Apoptosis assessed by flow cytometry. The induction of early and late apoptosis was analyzed by flow cytometry using the Becton Dickinson FACSCalibur flow cytometer (BD Biosciences). *JNK*$^{+/+}$, *JNK1*$^{-/-}$, and *JNK2*$^{-/-}$ MEFs or SK-MEL-28 cells (3×10^5 per dish) were grown in 6-cm dishes for 12 h in 10% FBS-DMEM (MEFs) or 10% FBS-MEM (SK-MEL-28 cells). Then, the cells were cultured in serum-free medium for 12 h and treated with UVA (40 kJ/m^2) in serum-free medium. After an additional incubation for 24 h, the medium was collected and attached cells were harvested with 0.025% trypsin in 5 mM EDTA in phosphate-buffered saline (PBS). The trypsinization was stopped by adding 2 ml of 5% FBS in PBS. The cells were washed by centrifugation at 1,000 rpm (170 relative centrifugal force) for 5 min and processed for the detection of early and late apoptosis using annexin V-fluorescein isothiocyanate (FITC) and propidium iodide staining according to the manufacturer's protocol. In brief, cells ($\sim 1 \times 10^5$ to $\sim 5 \times 10^5$) were collected after centrifugation and resuspended in 500 μl of 1× binding buffer (annexin V-FITC apoptosis detection kit; Medical & Biological Laboratories). Then, 5 μl of annexin V-FITC and 5 μl of propidium iodide were added, and the cells were incubated in the dark at room temperature for 5 min and analyzed by flow cytometry.

TUNEL assay. Late apoptotic events were analyzed by terminal deoxynucleotidyl transferase UTP nick end labeling (TUNEL) assay using an in situ cell death detection kit (Roche, Branchburg, New Jersey). Briefly, *JNK*$^{+/+}$, *JNK1*$^{-/-}$, and *JNK2*$^{-/-}$ MEFs or SK-MEL-28 cells were plated on glass coverslips in six-well plates at a concentration of 2×10^5 cells/ml. The next day, the cells were starved in serum-free medium for 12 h and then treated with UVA (40 kJ/m^2) in serum-free medium. After an additional incubation for 24 h, the TUNEL assay was performed according to the manufacturer's protocol (Roche). Apoptotic cells were visualized under an Axiovert 200 M fluorescence microscope and processed by AxioVision software (Carl Zeiss, Inc., Thornwood, NY). Each experiment was repeated three times independently of each other.

***Xenopus laevis* experiments.** Full-length human *Myt1* was inserted into a BglII/XbaI-digested pCS2-flag-tagged vector. mRNA synthesis and microinjection were performed as previously described (10, 49). Fertilized eggs were injected at the one-cell stage in the animal pole with mRNA. The embryos were then cultured until the gastrulation stage in 30% modified frog Ringer's buffer comprised of 0.1 M NaCl, 2 mM KCl, 2 mM $CaCl_2$, 1 mM $MgCl_2$, 5 mM HEPES (pH 7.6). The embryos, which were cultured until stage 40, were rinsed several times with 1× PBS, fixed for 1 h at room temperature in MEMFA (0.1 M MOPS [morpholinepropanesulfonic acid], 2 mM EGTA, 1 mM $MgSO_4$, 3.7% formaldehyde), and stored at 4°C in 100% methanol. The fixed embryos were observed and photographed under a microscope. Anti-Flag (Sigma-Aldrich, St. Louis, MO) was used for the detection of the equivalent expression of human Myt1 by immunoblotting analysis. The detection of α-tubulin was used as a loading control.

Tumor induction experiments. JNK1 knockout (*JNK1*$^{-/-}$) and JNK2 knockout (*JNK2*$^{-/-}$) mice were generated as described previously (10, 50). The WT, *JNK1*$^{-/-}$, and *JNK2*$^{-/-}$ mice were subsequently crossed with SKH-1 hairless mice to generate hairless strains of each JNK strain, including the WT. The genomic DNA phenotype and the protein expression of each respective SKH-1 hairless/JNK strain were confirmed by PCR and Western blotting. WT hairless JNK mice expressed both the JNK1 and JNK2 proteins, whereas the hairless *JNK1*$^{-/-}$ and *JNK2*$^{-/-}$ mice did not express the JNK1 and JNK2 proteins, respectively (data not shown). The expression of JNK1 and JNK2 in *JNK1*$^{-/-}$ and *JNK2*$^{-/-}$ mice, respectively, was unaffected, which is in agreement with our previous results (6, 39). Thus, the generation of hairless *JNK* WT, *JNK1*$^{-/-}$, and *JNK2*$^{-/-}$ mice was effective and specific, and these mice were used in the present experiments. The WT, *JNK1*$^{-/-}$, and *JNK2*$^{-/-}$ mice ($n = 30$ mice/group) were initiated once with DMBA and treated 5 days/week (Monday through Friday) with increasing doses of UVA irradiation. During week 1, each mouse received one daily dose of UVA at 4,200 J/m^2 on each of the 5 days; week 2, 8,400 J/m^2; week 3, 16,800 J/m^2; week 4, 33,600 J/m^2; week 5, 67,200 J/m^2; week 6, 100,800 J/m^2; and weeks 7 to 18, 144,000 J/m^2. Tumor development was monitored in these groups for 18 weeks.

RESULTS

JNK1 or JNK3 interacts with Myt1. To identify specific substrates for JNK1, JNK2, or JNK3, various potential protein-binding partners of each JNK protein were screened using the M2-H system (Promega). Among the 60 protein kinases screened, the human membrane-associated kinase Myt1 was found to interact with JNK1 and JNK3, but not JNK2, in vitro (data not shown). Based on the results of the M2-H assay, we next examined the in vitro interaction of Myt1 with JNK1, JNK2, or JNK3 by cotransfecting a Myt1 expression vector and the V5-tagged JNK1, JNK2, or JNK3 into HEK293 cells. The

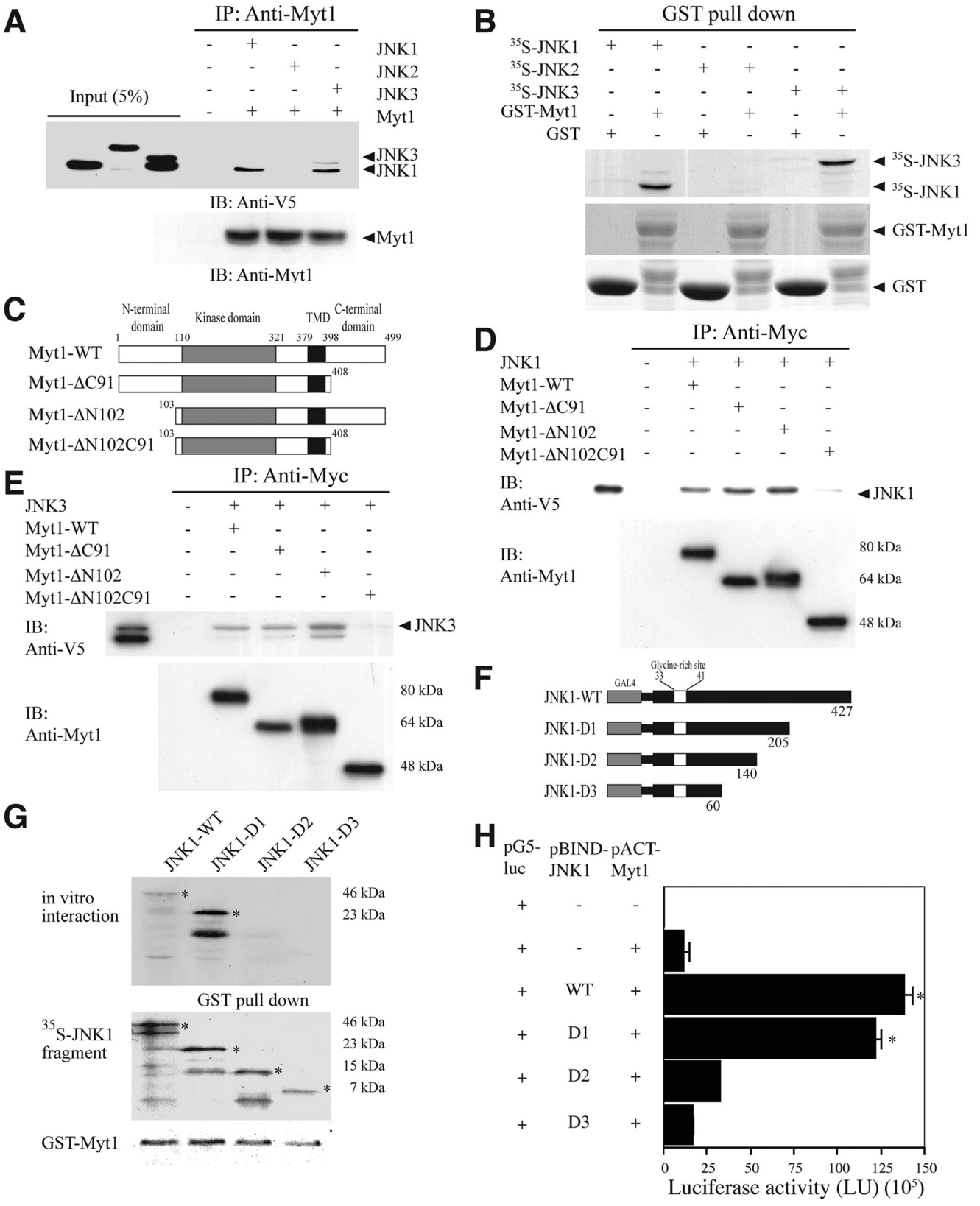
A
IP: Anti-Myt1
JNK1
JNK2
JNK3
Myt1
Input (5%)
JNK3
JNK1
IB: Anti-V5
Myt1
IB: Anti-Myt1
B
GST pull down
35S-JNK1
35S-JNK2
35S-JNK3
GST-Myt1
GST
35S-JNK3
35S-JNK1
GST-Myt1
GST
C
N-terminal domain
Kinase domain
TMD
C-terminal domain
Myt1-WT
Myt1-ΔC91
Myt1-ΔN102
Myt1-ΔN102C91
D
IP: Anti-Myc
JNK1
Myt1-WT
Myt1-ΔC91
Myt1-ΔN102
Myt1-ΔN102C91
IB: Anti-V5
JNK1
IB: Anti-Myt1
80 kDa
64 kDa
48 kDa
E
IP: Anti-Myc
JNK3
Myt1-WT
Myt1-ΔC91
Myt1-ΔN102
Myt1-ΔN102C91
IB: Anti-V5
JNK3
IB: Anti-Myt1
80 kDa
64 kDa
48 kDa
F
Glycine-rich site
GAL4
JNK1-WT
JNK1-D1
JNK1-D2
JNK1-D3
G
JNK1-WT
JNK1-D1
JNK1-D2
JNK1-D3
in vitro interaction
46 kDa
23 kDa
GST pull down
35S-JNK1 fragment
46 kDa
23 kDa
15 kDa
7 kDa
GST-Myt1
H
pG5-luc
pBIND-JNK1
pACT-Myt1
WT
D1
D2
D3
0 25 50 75 100 125 150
Luciferase activity (LU) (10^5)

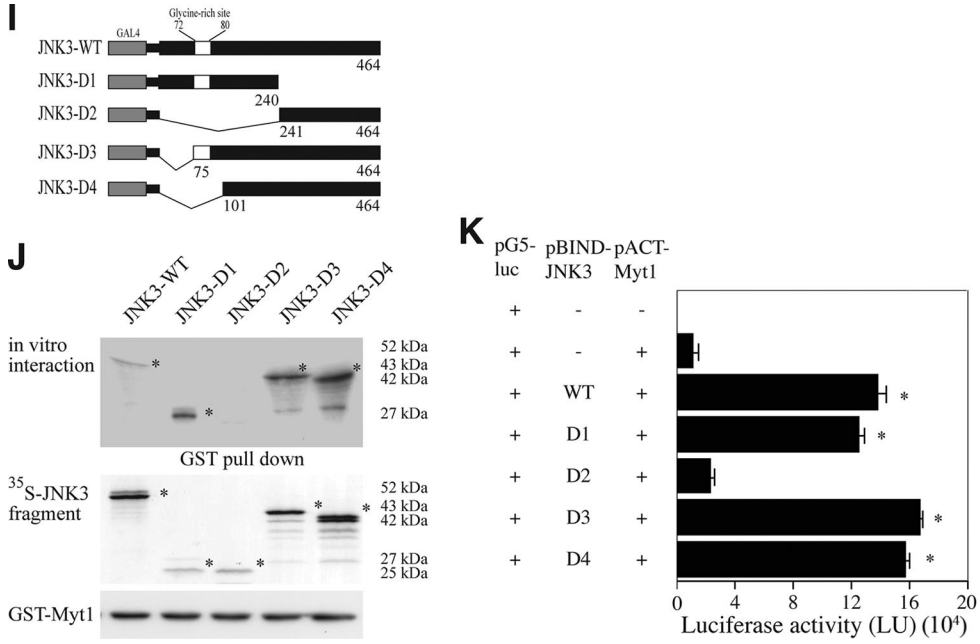

FIG. 1. The interaction of Myt1 with the JNK proteins. (A) JNK1, JNK2, or JNK3 was coimmunoprecipitated with Myt1. The pcDNA3-V5-JNK1, -JNK2, or -JNK3 plasmid was cotransfected with pcDNA3-myc-Myt1 into HEK293 cells and then cultured for 48 h at 37°C in a 5% CO_2 incubator. Cells transfected with the pcDNA3-mock vector served as a negative control. The proteins were extracted as described in Materials and Methods and were used for immunoprecipitation (IP) with anti-myc. JNK1, JNK2, and JNK3 were visualized by Western blotting with anti-V5 horseradish peroxidase followed by detection using an ECL detection kit (Amersham Biosciences). (B) In vitro binding with ^{35}S-labeled JNK proteins and a GST-Myt1 fusion protein. The cDNA of each JNK protein was translated in vitro, and then the ^{35}S-JNK proteins were mixed with GST-Myt1 and a pulldown assay was performed. Proteins were visualized by autoradiography. (C) Schematic diagram of full-length (residues 1 to 499) myc-Myt1 (Myt1-WT), the N-terminal fragment (residues 1 to 408) of myc-Myt (Myt1-ΔC91), the C-terminal fragment (residues 103 to 499) of myc-Myt1 (Myt1-ΔN102), or the kinase domain fragment (residues 110 to 321) of myc-Myt1 (Myt1-ΔN102C91). (D and E) The pcDNA3-myc-Myt1-WT, -ΔC91, -ΔN102, or -ΔN102ΔC91 plasmid was transfected with pcDNA3-V5-JNK1 (D) or pcDNA3-V5-JNK3 (E) into HEK293 cells and then cultured for 48 h at 37°C in a 5% CO_2 incubator. The cells transfected with the pcDNA3-mock vector served as a negative control. The proteins were extracted as described in Materials and Methods and were used for IP with anti-Myc. JNK1 and JNK3 were visualized by Western blotting with anti-V5 horseradish peroxidase followed by detection using an ECL detection kit (Amersham Biosciences). (F) Schematic diagram of full-length (residues 1 to 427) V5-JNK1 (JNK1-WT) or various deletion mutants of V5-JNK1 (JNK1-D1 [residues 1 to 205], JNK1-D2 [residues 1 to 140], and JNK1-D3 [residues 1 to 60]). (G) In vitro binding with ^{35}S-labeled JNK1-WT or various deletion mutants (JNK1-D1, -D2, or -D3) and a GST-Myt1 fusion protein. The cDNA of JNK1-WT or the deletion mutants (JNK1-D1, -D2, or -D3) was translated in vitro, and then the ^{35}S-labeled JNK1-WT or each respective deletion mutant protein was mixed with GST-Myt1 and a pulldown assay was performed. Proteins were visualized by autoradiography. (H) Ex vivo interaction of pACT-Myt1 with pBIND full-length JNK1 (residues 1 to 427) or each respective deletion mutant. For a negative control, the pACT-Myt1 plasmid was transfected along with the pG5-*luc* reporter plasmid into NIH 3T3 cells (18,000 cells/ml). The pACT-Myt1 and pBIND-JNK1 plasmids (WT, D1, D2, or D3) were cotransfected with the pG5-*luc* plasmid to confirm the binding site of Myt1 with JNK1. After a 36-h incubation, the firefly luciferase activity was determined in the cell lysates and normalized against *Renilla* luciferase activity. All of the experiments were performed at least twice with triplicate samples and are depicted as the means ± standard errors (S.E.). The asterisks indicate a significant increase in activity compared to that for the negative control, pACT-Myt1 only ($P < 0.05$). The data are shown as relative luciferase activity units (LU) as measured by a Luminoskan Ascent plate reader (Thermo Electron Corp., Helsinki, Finland). (I) Schematic diagram of full-length (residues 1 to 464) V5-JNK3 (JNK1-WT) or various deletion mutants of V5-JNK3 (JNK3-D1 [residues 1 to 240], JNK3-D2 [residues 241 to 464], JNK3-D3 [residues 75 to 464], and JNK3-D4 [residues 101 to 464]). (J) In vitro binding with ^{35}S-labeled JNK3-WT or various deletion mutants (JNK3-D1, -D2, -D3, or -D4) and a GST-Myt1 fusion protein. The cDNA of JNK3-WT or each respective deletion mutant (JNK3-D1, -D2, -D3, or -D4) was translated in vitro; then, the ^{35}S-labeled JNK3-WT or individual deletion mutant protein was mixed with GST-Myt, and a pulldown assay was performed. Proteins were visualized by autoradiography. (K) Ex vivo interaction of pACT-Myt1 with pBIND full-length JNK3 (residues 1 to 464) or each respective deletion mutant. For a negative control, the pACT-Myt1 plasmid was transfected along with the pG5-*luc* reporter plasmid into NIH 3T3 cells (18,000 cells/ml). The pACT-Myt1 and pBIND-JNK3 plasmids (WT, D1, D2, D3, or D4) were cotransfected with the pG5-*luc* plasmid to confirm the binding site of Myt1 with JNK3. After a 36-h incubation, firefly luciferase activity was determined in the cell lysates and normalized against *Renilla* luciferase activity. All of the experiments were performed at least twice with triplicate samples and are depicted as means ± S.E. The asterisks indicate a significant increase in activity compared to that for the negative control, pACT-Myt1 only ($P < 0.05$). The data are shown as relative luciferase activity units (LU) as measured by a Luminoskan Ascent plate reader (Thermo Electron Corp., Helsinki, Finland).

results indicated that exogenous Myt1 interacted with JNK1 and JNK3 but not JNK2 (Fig. 1A). In addition, a GST-Myt1 fusion protein was incubated with a ^{35}S-labeled JNK1, JNK2, or JNK3 protein. We detected ^{35}S-labeled JNK1 or JNK3 together with GST-Myt1 in an immunoprecipitation assay, suggesting that Myt1 physically interacted with JNK1 or JNK3, but not JNK2, in vitro (Fig. 1B). To determine the region of Myt1 that was responsible for its interaction with JNK1 or JNK3, full-length Myt1 (Myt1-WT), a C-terminal deletion mutant (Myt1-ΔC91), an N-terminal deletion mutant (Myt1-ΔN102), or a double-terminal deletion (Myt1-ΔN102C91) mutant (Fig. 1C) was cotransfected with JNK1 (Fig. 1D) or JNK3 (Fig. 1E), respec-

tively, and the interaction was examined by an immunoprecipitation assay. The results suggested that both the N-terminal and the C-terminal ends of Myt1 were required for its interaction with JNK1 (Fig. 1D) or JNK3 (Fig. 1E). Next, the specific site of the interaction of JNK1 or JNK3 with Myt1 was assessed by both an immunoprecipitation assay (Fig. 1G or 1J) and the M2-H assay (Fig. 1H or K). JNK1 (pcDNA3.1/V5-JNK1 or pBIND-JNK1) or each respective JNK1 deletion fragment (pcDNA3.1/V5-JNK1 or pBIND-JNK1 WT, D1, D2, or D3) was cotransfected with full-length Myt1 (pCS3-myc- or pACT-Myt1) into HEK293 cells. The results showed that residues 140 to 205 of JNK1 have the ability to interact with Myt1 (Fig. 1G or H). In the case of JNK3, we transfected JNK3 (pcDNA3.1/V5-JNK3 or pBIND-JNK3) or each respective JNK3 deletion fragment (pcDNA3.1/V5-JNK3 or pBIND-JNK3 WT, D1, D2, D3, or D4) along with full-length Myt1 (pCS3-myc- or pACT-Myt1) into HEK293 cells. In this case, residues 1 to 240 of JNK3 were shown to interact with Myt1 (Fig. 1J or K). These results indicated that JNK1 or JNK3 selectively interacts with Myt1 at distinct amino acid sequences.

JNK1 or JNK3 mediates the phosphorylation of Myt1. Myt1 is a dual-specificity kinase involved in the regulation of the eukaryotic cell cycle (12, 25). It is responsible for the inhibitory phosphorylation of the Cdk/cyclin complexes on adjacent Thr14 and Tyr15 sites located near the ATP-binding pocket of the Cdk subunit (31). Because of the observed physical interaction between JNK1 and Myt1 (Fig. 1), we investigated whether JNK1 or JNK3 might function to regulate Myt1 by phosphorylation. A kinase assay using GST-Myt1 revealed that active JNK1 or JNK3, but not JNK2, phosphorylated Myt1 in vitro (Fig. 2A). On the other hand, all three of the active JNKs phosphorylated c-Jun in vitro (data not shown). Also, we confirmed that JNK1 was shown to phosphorylate Myt1 in SK-MEL-28 cells in a time-dependent manner following UVA irradiation (Fig. 2B). To determine whether endogenous JNK1 and Myt1 also interact ex vivo, we examined a time course for the UVA-induced interaction of JNK1 and Myt1 in human melanoma SK-MEL-28 cells. An antibody against JNK1 was used to immunoprecipitate JNK1, and then Myt1 was detected by immunoblotting. The results indicated that Myt1 was detectable from 3 to 9 h after UVA exposure in JNK1 immunoprecipitates (Fig. 2C). However, in SK-MEL-28 cells, JNK2 did not bind with Myt1 at 6 h after UVA exposure, which is the strongest time point for JNK1 to interact with Myt1 (Fig. 2D). Next, we determined whether the phosphorylation of Myt1 induced by UVA has effects on the well-established substrate CDK1 in JNK-deficient MEFs. We found a substantially increased phosphorylation of Myt1 from 1 to 3 h in $JNK^{+/+}$or $JNK2^{-/-}$ MEFs (Fig. 2E). The phosphorylation of CDK1 (Tyr15) was also increased accordingly. In contrast, the phosphorylation of Myt1 and CDK1 (Tyr15) was attenuated in $JNK1^{-/-}$ MEFs (Fig. 2E). Taken together, these results indicated that UVA-activated JNK1 could interact with and phosphorylate Myt1.

JNK1 deficiency prevents UVA-induced apoptosis. Tournier et al. (44) reported that UV induces apoptosis through the JNK/cytochrome *c*/caspase-3 pathway. To examine whether UVA-induced apoptosis is regulated through the JNK1-Myt1 signaling pathway, we exposed $JNK^{+/+}$, $JNK1^{-/-}$, or $JNK2^{-/-}$ MEFs to UVA (40 kJ/m^2) and examined the effect on various proteins. We found a substantially increased cleavage of caspase-3 from 2 to 3 h or from 2 to 6 h in $JNK^{+/+}$or $JNK2^{-/-}$ MEFs, respectively (Fig. 3A). The phosphorylation of Myt1 was also increased accordingly. In contrast, caspase-3 cleavage and Myt1 phosphorylation were attenuated in $JNK1^{-/-}$ MEFs (Fig. 3A). Next, we examined differences in UVA-induced apoptosis in $JNK^{+/+}$, $JNK1^{-/-}$, or $JNK2^{-/-}$ MEFs by flow cytometry analysis. UVA induced the apoptosis of $JNK^{+/+}$ and $JNK2^{-/-}$ MEFs (Fig. 3B), as characterized by a markedly high rate of total apoptosis of 48% (Fig. 3C) and a sub-G_1 cell population that reached 50% (Fig. 3D) in the $JNK^{+/+}$ MEFs and 90% and 99%, respectively, in the $JNK2^{-/-}$ MEFs after UVA exposure. In contrast, the $JNK1^{-/-}$ MEFs were highly resistant to UVA-induced apoptosis (Fig. 3B to D). To further confirm these results, we next examined UVA-induced DNA fragmentation in $JNK^{+/+}$, $JNK1^{-/-}$, or $JNK2^{-/-}$ MEFs using the TUNEL assay. The results indicated that UVA-induced DNA fragmentation was substantially inhibited in $JNK1^{-/-}$ MEFs compared to that observed in either $JNK^{+/+}$ or $JNK2^{-/-}$ MEFs (Fig. 3E). Overall, these data provide strong evidence indicating that JNK1-induced Myt1 phosphorylation is required for caspase-3 cleavage and DNA fragmentation resulting in cellular apoptosis after exposure to UVA.

The knockdown of Myt1 suppresses UVA-induced apoptosis. Next, to confirm the role of Myt1 in UVA-induced apoptosis, we examined apoptosis in human Myt1 knockdown cells by exposing SK-MEL-28 cells, which expressed either control siRNA or siRNA against Myt1, to UVA (40 kJ/m^2). UVA induced the phosphorylation of Myt1 and JNK1/2 from 6 h to 9 h in control siRNA-transfected cells, corresponding with increased caspase-3 cleavage (Fig. 4A, left panels). However, Myt phosphorylation and caspase-3 cleavage were markedly inhibited in Myt1 knockdown cells (Fig. 4A, right panels). Next, we examined the cell viability and activated caspase-3 in Myt1-ΔN102C91-overexpressing cells, which attenuates its interaction with JNK1, by exposing SK-MEL-28 cells to UVA (40 kJ/m^2). UVA inhibited cell viability and activated caspase-3 in Myt1-WT-overexpressing cells, but not in Myt1-ΔN102C91-overexpressing cells, compared with results for the control cells, suggesting that its interaction with JNK1 may play an important role in Myt1-induced apoptosis (Fig. 4B). Furthermore, UVA induced the apoptosis of control siRNA-transfected SK-MEL-28 cells, which was characterized by a marked rate of total apoptosis that reached 37% at 12 h after UVA exposure (Fig. 4C [top panels] and D). In contrast, Myt1 siRNA-transfected cells were highly resistant to UVA-induced apoptosis (Fig. 4C [bottom panels] and D). These results were confirmed by TUNEL analysis in control siRNA- and Myt1 siRNA-transfected cells exposed to UVA. UVA-induced DNA fragmentation was suppressed in Myt1 knockdown SK-MEL-38 cells, whereas UVA dramatically induced DNA fragmentation in control cells (Fig. 4E). Together, these data indicated that UVA-induced Myt1 phosphorylation is associated with apoptosis mediated through caspase-3 cleavage and DNA fragmentation in SK-MEL-28 cells, which is inhibited by the knockdown of Myt1.

The overexpression of Myt1 in *Xenopus* embryos induces apoptosis. To further study apoptosis mediated by Myt1, we investigated potential phenotypic changes in the *Xenopus* embryo system induced by the expression of Myt1. RNA encoding

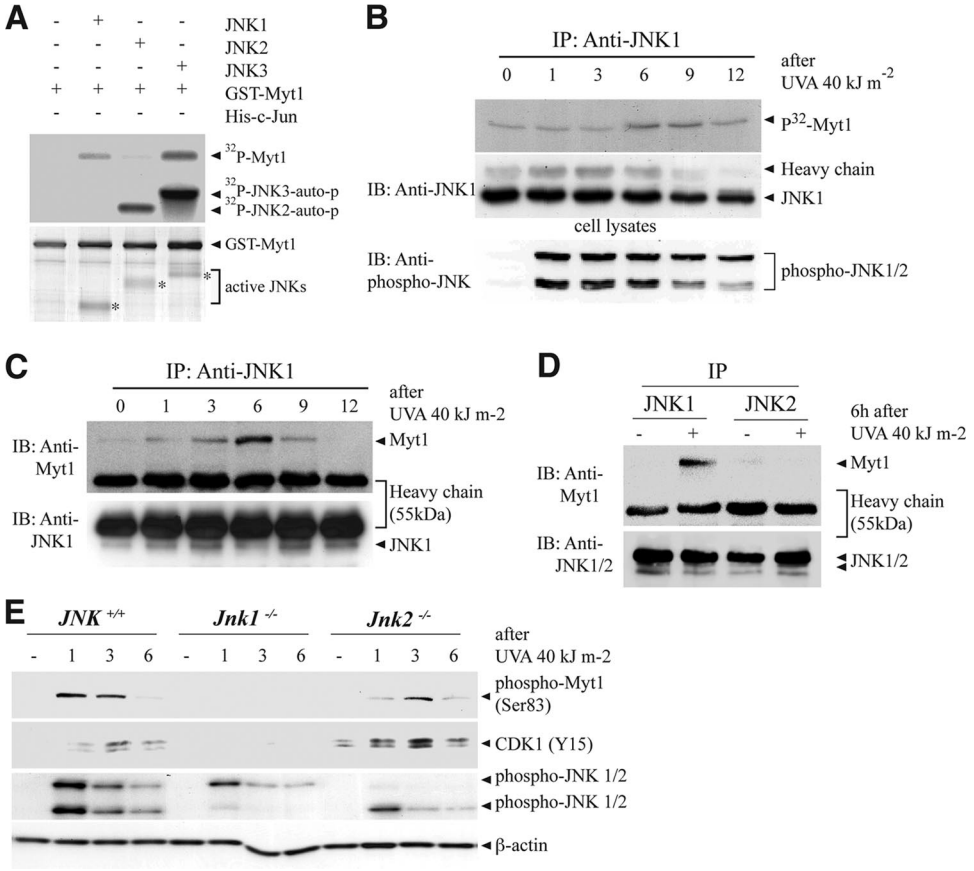

FIG. 2. JNK1 mediates the UVA-induced phosphorylation of Myt1. (A) In vitro phosphorylation of GST-Myt1 by active JNK1, JNK2, or JNK3. A GST-Myt1 protein was incubated with active JNK1, JNK2, or JNK3 protein (1 μg) for 60 min at 30°C for an in vitro kinase assay, and the ^{32}P-labeled Myt1 was visualized by autoradiography. For visualizing the equal loading of protein, total GST-Myt1 was detected by Coomassie blue staining (bottom panel). The figures are representative of at least two separate experiments that yielded similar results. auto-p, autophosphorylation. (B) In vitro phosphorylation of GST-Myt1 by UVA-induced JNK1 activation. SK-MEL-28 cells were seeded and cultured for 24 h in 10% FBS-MEM in a 37°C, 5% CO_2 incubator. The cells were then starved in serum-deprived MEM for 24 h, exposed or not exposed to UVA (40 kJ/m^2), and harvested after incubation for the time indicated. Immunoprecipitation (IP) was performed to precipitate endogenous JNK1, and then the GST-Myt1 protein was incubated with the immunoprecipitated active JNK1 protein for 60 min at 30°C for an in vitro kinase assay and the ^{32}P-labeled Myt1 was visualized by autoradiography. For visualizing UVA-induced JNK activity, the phosphorylation of JNKs was detected by immunoblotting (IB) using the total cell lysate (bottom panel). (C and D) Interaction of endogenous JNK1 or JNK2 with Myt1 stimulated by UVA. SK-MEL-28 cells were seeded and cultured for 24 h in 10% FBS-MEM in a 37°C, 5% CO_2 incubator. The cells were then starved in serum-deprived MEM for 24 h, then exposed or not exposed to UVA (40 kJ/m^2), and harvested after incubation for the time indicated (C) or 6 h (D). IP was performed to precipitate endogenous JNK1 (C or D) or JNK2 (D), and then the Myt1 protein was detected by IB with anti-Myt1. (E) The effect of the UVA-induced phosphorylation of Myt1 on CDK activity after JNK gene ablation. *JNK*$^{+/+}$, *JNK1*$^{-/-}$, or *JNK2*$^{-/-}$ MEFs were seeded and cultured for 24 h in 10% FBS-MEM in a 37°C, 5% CO_2 incubator and then starved in serum-deprived MEM for 24 h. Cells treated or not treated with UVA (40 kJ/m^2) for the indicated times were harvested, lysed, and resolved by SDS-PAGE. Western blot analysis was carried out using antibodies against the respective proteins.

Myt1 was synthesized and injected into embryos at the one-cell stage. The control embryos were injected with equal amounts of mRNA encoding a β-galactosidase (β-Gal) protein (Fig. 5A). During gastrulation, β-Gal mRNA-injected embryos developed normally (Fig. 5B, control panel). However, human Myt1 mRNA-injected embryos typically showed a delayed developmental stage (Fig. 5B, Type A and Type B panels) or cell dissociation (Fig. 5B, Type C panel) compared with that of the β-Gal mRNA-injected embryos (Fig. 5B, control panel). These phenotypes were induced in a dose-dependent manner (Fig. 5C). In particular, embryos showing the appearance of dissociated cells eventually underwent death and the cessation of development. These phenotypes were observed with doses of human Myt1 mRNA as low as 25 pg, and maximal effects were noted with 100 pg. The majority (~90%) of embryos expressing 100 pg of Myt1 exhibited cell death (Fig. 5C). This morphological change was entirely consistent with changes associated with apoptosis, as documented previously for *Xenopus* embryos (4, 18, 40, 42). To further confirm whether Myt1 triggers apoptotic cell death, embryos expressing β-Gal or Myt1 were analyzed by whole-mount TUNEL assays during gastrulation. The control embryos injected with β-Gal showed very few and weakly stained TUNEL-positive cells, whereas 80 to 100% of the embryos injected with Myt1 showed strong and positive TUNEL staining (Fig. 5D). Next, we examined the effect of dominant negative JNK1 (DN-JNK1) on Myt1-induced apoptotic cell death in *Xenopus* embryos. Human Myt1 mRNA-injected embryos typically showed 80% cell dissocia-

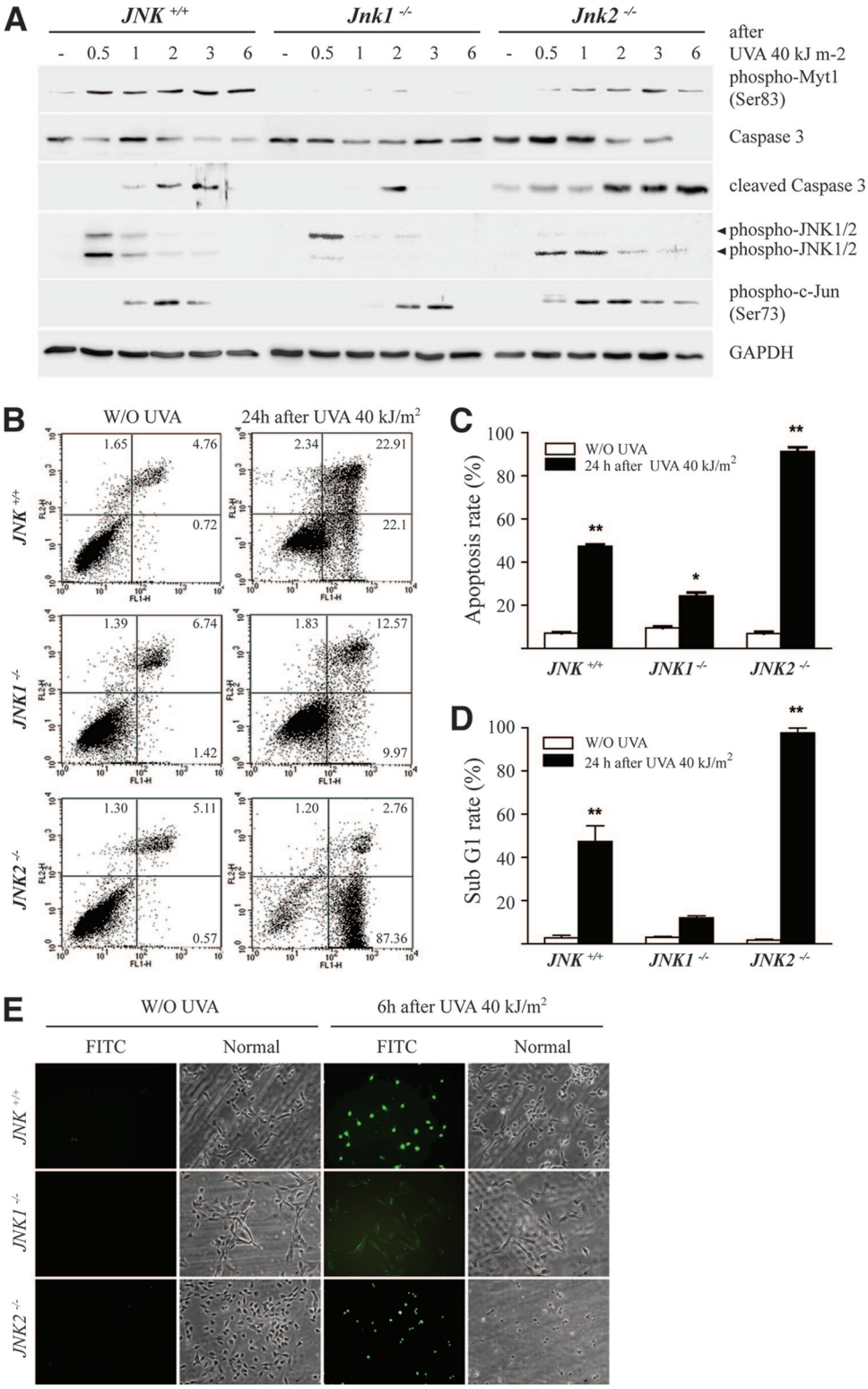

FIG. 3. JNK1 deficiency causes a reduction in cellular apoptosis. (A) Time-course analysis of the UVA-induced phosphorylation of Myt1 after gene ablation. $JNK^{+/+}$, $JNK1^{-/-}$, or $JNK2^{-/-}$ MEFs were seeded and cultured for 24 h in 10% FBS-MEM in a 37°C, 5% CO_2 incubator and then starved in serum-deprived MEM for 24 h. Cells treated or not treated with UVA (40 kJ/m^2) for the indicated times were harvested, lysed, and resolved by SDS-PAGE. Western blot analysis was carried out using antibodies against the respective proteins. (B) Flow cytometry analysis of UVA-induced apoptosis of $JNK^{+/+}$, $JNK1^{-/-}$, or $JNK2^{-/-}$ MEFs. Cells were incubated with annexin V-FITC and propidium iodide 24 h after treatment with UVA (40 kJ/m^2). Untreated cells were used as controls. The distribution pattern of the live and apoptotic cells was analyzed by flow cytometry using the Becton Dickinson FACSCalibur flow cytometer, as described in Materials and Methods. In the bottom left quadrants of each plot, viable cells are those displaying low annexin or no annexin and propidium iodide staining. In the bottom right quadrants, early-stage

tion, whereas the coinjection of DN-JNK1 mRNA decreased embryos showing the appearance of disassociated cells by Myt1 (Fig. 5E). To determine the role of JNK1 or JNK2 in Myt1-induced cellular apoptosis in *Xenopus* embryos, the embryos were overexpressed with Myt1 in the presence of JNK1 or JNK2. The overexpression of JNK1 with Myt1 enhances apoptotic cell death in *Xenopus* embryos (Fig. 5F [top panels] and G), whereas the overexpression of JNK2 suppresses the phenotype of Myt1-induced apoptotic cell death (Fig. 5F [bottom panels] and H). Taken together, these data suggest that apoptotic cell death in *Xenopus* embryos is augmented by the overexpression of JNK1, but not JNK2, with Myt1 simultaneously.

UVA-promoted tumor development in JNK-deficient mice. To induce tumor formation in the skin of JNK-deficient mice, we used a classical multistage model in which tumors were initiated with DMBA and promoted with UVA. DMBA (200 nmol) was topically applied in acetone (250 μl). Two weeks later, the mice were exposed to increasing doses of UVA 5 times a week for 18 weeks. The first papillomas were observed at 5 weeks for $JNK1^{-/-}$ and $JNK2^{-/-}$ mice but not until 7 weeks for $JNK^{+/+}$ mice. The development of papillomas in $JNK^{+/+}$ mice lagged behind both $JNK1^{-/-}$ and $JNK2^{-/-}$ papilloma development until week 9, when $JNK^{+/+}$ tumor development passed $JNK2^{-/-}$ development. By week 14, 100% of the $JNK1^{-/-}$ and $JNK^{+/+}$ mice had developed papillomas, whereas only 65.5% of the $JNK1^{-/-}$ mice had developed papillomas. At the end of the study (18 weeks), only 75.9% of the $JNK1^{-/-}$ mice had developed papillomas (Fig. 6B). Following chronic exposure to UVA, the $JNK2^{-/-}$ mice developed fewer papillomas than either the $JNK1^{-/-}$ or $JNK^{+/+}$ mice, and the $JNK1^{-/-}$ mice developed more papillomas than either the $JNK2^{-/-}$ or $JNK^{+/+}$ mice (Fig. 6C). With chronic exposure to UVA, fewer $JNK2^{-/-}$ mice than $JNK^{+/+}$ or $JNK1^{-/-}$ mice developed papillomas that were >1.5 mm^3, and more $JNK1^{-/-}$ mice than $JNK^{+/+}$ or $JNK2^{-/-}$ mice developed papillomas that were >1.5 mm^3 (Fig. 6D). We also observed that $JNK2^{-/-}$ mice developed papillomas smaller than those of the $JNK1^{-/-}$ or $JNK^{+/+}$ mice and that $JNK1^{-/-}$ mice developed papillomas larger than those of either the $JNK2^{-/-}$ or $JNK^{+/+}$ mice following chronic exposure to UVA (Fig. 6E). These data strongly support the idea that a deficiency of the *JNK1* gene increases the formation and growth of DMBA/UVA-induced skin tumors and therefore that JNK1 and its various substrates might act as tumor suppressors. To further explore the idea as to whether skin cancer development is regulated by the JNK1–Myt1–caspase-3 signaling pathway, skin samples from $JNK^{+/+}$, $JNK1^{-/-}$, or $JNK2^{-/-}$ mice from the 18-week study were biopsied, and the total lysates were analyzed by immunoblotting. We found that caspase-3 cleavage and Myt1 phosphorylation induced by UVA were markedly suppressed in $JNK1^{-/-}$ mice compared to levels in the $JNK^{+/+}$ *or* $JNK2^{-/-}$ mice (Fig. 6F, top two panels, respectively). Interestingly, levels of DMBA/UVA-induced c-Jun phosphorylation were not really different in any of the three strains of mice, suggesting that changes in c-Jun phosphorylation are not associated with UVA-induced apoptosis or skin cancer (Fig. 6F, middle panel). Our results suggest that the marked decrease in caspase-3 cleavage mediated in $JNK1^{-/-}$ mice, which is increased in $JNK^{+/+}$ or $JNK2^{-/-}$ mice, may be an alternative mechanism that may account for the observed greater tumorigenicity in $JNK1^{-/-}$ mice (Fig. 6A) than in WT or $JNK2^{-/-}$ mice.

DISCUSSION

Many components of cellular signaling modules, including the JNK proteins, are encoded by multiple evolutionarily conserved genes, the protein products of which exhibit common modes of regulation (3). However, whether structurally similar molecules have similar or distinct biological functions is still a question to be addressed. We have shown here that despite their biochemical and structural similarities, JNK1 and JNK2 exert dissimilar effects in the development of skin cancer, which correspond with their differential effects on cellular apoptosis. In particular, JNK1, but not JNK2, appears to be a positive regulator of cellular apoptosis and is required for the phosphorylation of Myt1, which mediates UVA-induced caspase-3 cleavage and DNA fragmentation.

JNKs have been reported to be constitutively activated in several tumor cell lines and the transforming actions of several oncogenes were suggested to be JNK dependent (20). In addition, the $p16^{INK4a}$ protein, an important tumor suppressor, was reported to inhibit the activity of JNK proteins induced by UV exposure, suggesting that tumorigenesis promoted by the H-Ras–JNK–c-Jun–AP-1 signaling axis is deterred by the interaction of $p16^{INK4a}$ with JNKs (7). On the other hand, the double knockout of JNK ($JNK1^{-/-}/JNK2^{-/-}$) in fibroblasts was reported to cause marked increases in the number and growth of Ras-induced tumor nodules in vivo, suggesting that

apoptotic cells are represented by high annexin and low propidium iodide staining. In the top right quadrants, late-stage apoptotic cells are represented by high annexin and high propidium iodide staining. In the top left quadrants, necrosis is represented by cells with high propidium iodide and low annexin staining. These data are representative of the results from at least three independent experiments. (C) Percentage of apoptosis in UVA-treated cells compared with that of the untreated cells. Data are represented as the means of the results from three independent experiments ± standard deviations (S.D.). The asterisks indicate a significant increase in apoptosis induced by UVA compared with that of the untreated control cells (*, $P < 0.005$; **, $P < 0.001$). (D) Effect of UVA on the sub-G_1 distribution of $JNK^{+/+}$, $JNK1^{-/-}$, or $JNK2^{-/-}$ MEFs. Cells were seeded and allowed to attach overnight. Cells were then exposed to UVA (40 kJ/m^2), and 24 h later, total cells (floating and attached) were fixed, stained with propidium iodide, and analyzed by flow cytometry. The percentage of cell staining with <2 N DNA content (sub-G_1) for UVA-treated cells was compared with that for untreated cells. Data are represented as the means of the results from three independent experiments ± S.D. The asterisks indicate a significant increase in the distribution of sub-G_1 cells induced by UVA compared with that for untreated control cells (**, $P < 0.001$). (E) TUNEL analysis of UVA-induced apoptosis in $JNK^{+/+}$, $JNK1^{-/-}$, or $JNK2^{-/-}$ MEFs. Apoptosis was evaluated by the TUNEL assay as a measure of DNA fragmentation. Cells were exposed or not exposed to UVA (40 kJ/m^2) and harvested 6 h later as described in Materials and Methods. Large numbers of TUNEL-positive cells were observed in $JNK^{+/+}$ and $JNK2^{-/-}$ MEFs, but not in $JNK1^{-/-}$ cells, after UVA exposure. Reproducible results were obtained in three independent experiments, and representative photomicrographs are shown.

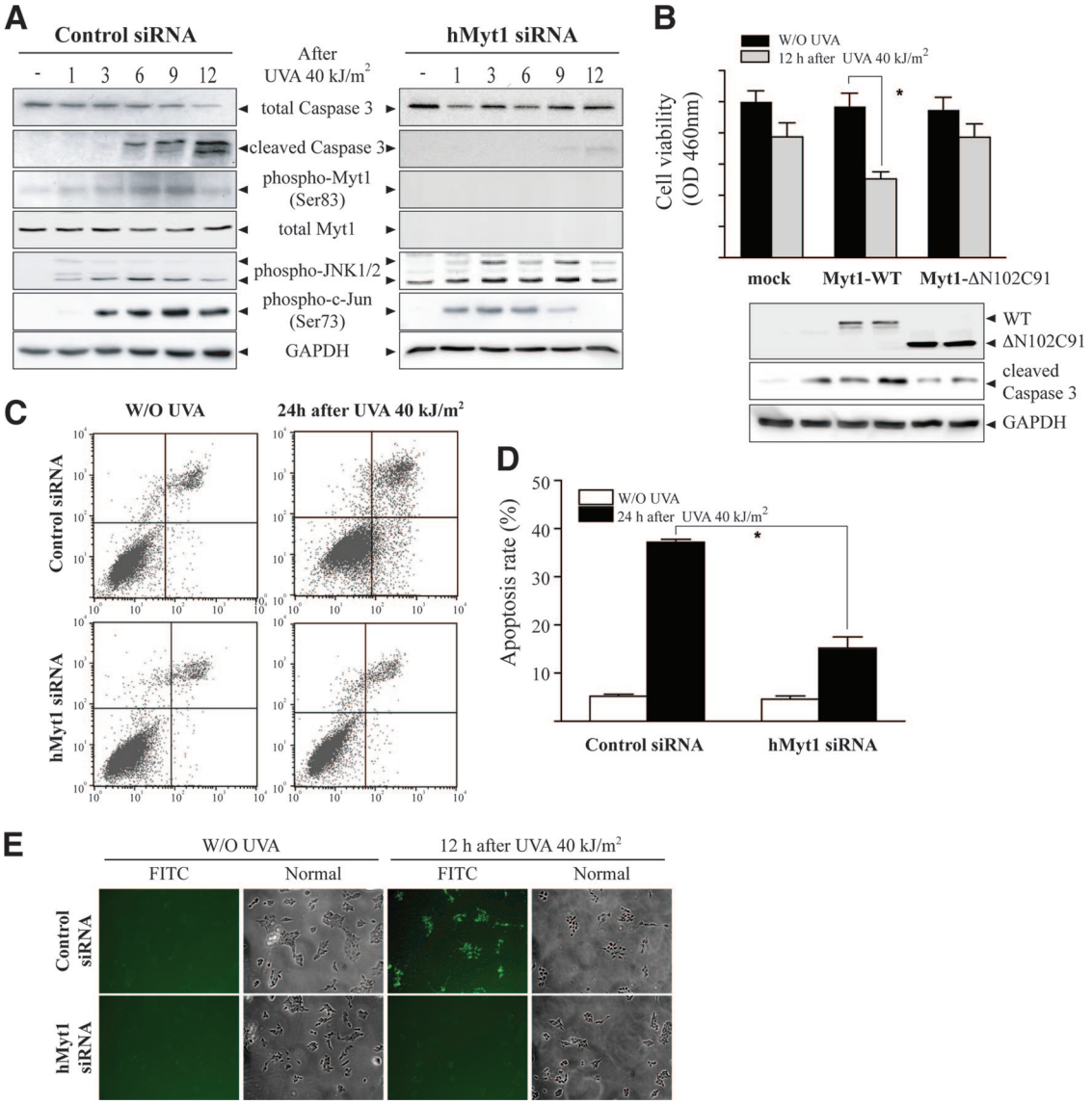

FIG. 4. Myt1 knockdown inhibits UVA-induced cellular apoptosis. (A) Time-course analysis of the UVA-induced signaling to apoptosis in Myt1 knockdown SK-MEL-28 cells. Cells were seeded and cultured for 24 h in 10% FBS-MEM in a 37°C, 5% CO_2 incubator and then transfected with siRNA against human Myt1 (hMyt1). At 24 h after the transfection of hMyt1 siRNA, cells were starved for an additional 24 h, then treated or not treated with UVA (40 kJ/m^2), and harvested at the indicated time point. Cells were disrupted and proteins resolved by SDS-PAGE. Western blot analysis was carried out using antibodies against the respective proteins. (B) Comparison of cell viability and caspase-3 activation stimulated by UVA in Myt1-WT- or Myt1-ΔN102C91-overexpressing SK-MEL-28 cells. Cells were seeded and cultured for 24 h in 10% FBS-MEM in a 37°C, 5% CO_2 incubator and then transfected with the mock vector, Myt1-WT, or Myt1-ΔN102C91, respectively. At 24 h after transfection, cells were starved for an additional 24 h, then treated or not treated with UVA (40 kJ/m^2), and incubated for 12 h. Cells were harvested and disrupted and proteins resolved by SDS-PAGE. Western blot analysis was carried out using antibodies against the respective proteins. (C) Flow cytometry analysis of UVA-induced apoptosis in control siRNA- or hMyt1 siRNA-transfected cells. Cells transfected with control siRNA or hMyt1 siRNA were incubated with annexin V-FITC and propidium iodide 24 h after treatment with UVA (40 kJ/m^2). Untreated cells were used as controls. The distribution pattern of live and apoptotic cells was analyzed by flow cytometry using the Becton Dickinson FACSCalibur flow cytometer, as described in Materials and Methods. These data are representative of the results from at least three independent experiments. (D) The percentage of apoptosis in UVA-treated cells is compared with that for untreated cells, and the data represent the means ± standard deviations of the results from three independent experiments. The asterisks indicate a significant decrease in apoptosis induced by UVA in hMyt1 siRNA-treated cells compared with that in control siRNA-treated cells (*, $P < 0.005$). (E) TUNEL analysis of UVA-induced apoptosis in control siRNA- or hMyt1 siRNA-transfected cells. Apoptosis was evaluated by the TUNEL assay as a measure of DNA fragmentation. Control siRNA- or hMyt1 siRNA-transfected cells were exposed or not exposed to UVA (40 kJ/m^2) and harvested after 12 h as described in Materials and Methods. Substantially more TUNEL-positive cells were observed for control siRNA-transfected SK-MEL-28 cells after exposure to UVA than for hMyt1-transfected SK-MEL-28 cells. Reproducible results were obtained from three independent experiments, and representative photomicrographs are shown.

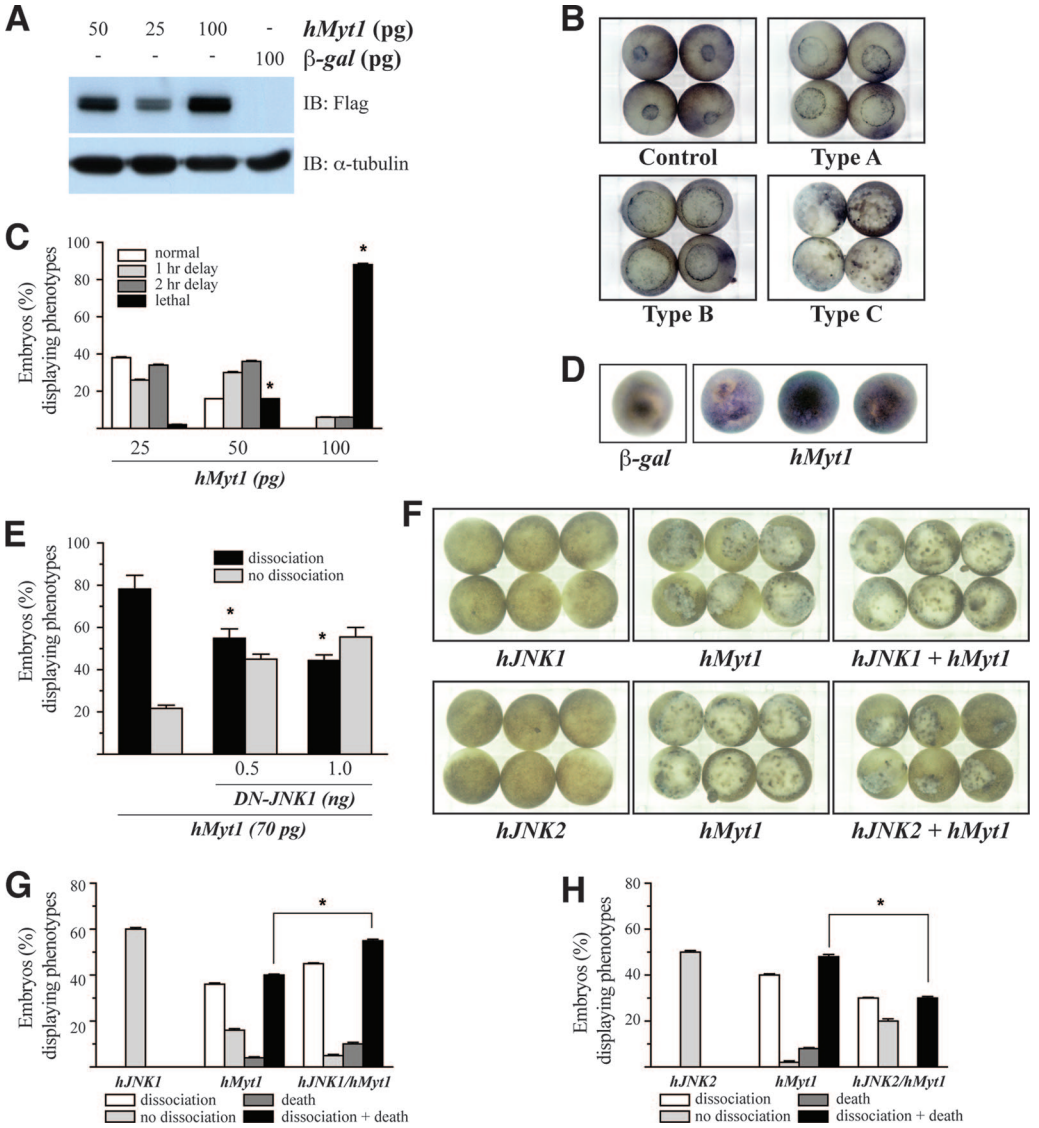

FIG. 5. Overexpression of Myt1 results in apoptosis during gastrulation. (A) *Xenopus* embryos were injected at the one-cell stage with the mRNA of Myt1 at the indicated dose or 100 pg of β-Gal (negative control). Embryos were collected, and lysates were subjected to immunoblotting using anti-Flag. (B) *Xenopus* embryos injected with the mRNA of β-Gal or human Myt1 were photographed. Control, normal embryos at stage 12 derived from one-cell-stage embryos that were injected with the mRNA of β-Gal (100 pg) as a control; Type A, Type B, and Type C, embryos derived from one-cell-stage embryos that were injected with the mRNA of Myt1. The types of embryos were classified as type A, type B, or type C based on the severity of the phenotypic defect. (C) Histogram representing the number of phenotypic changes induced by Myt1. The asterisks indicate a significant increase in lethality compared to that for the control ($P < 0.05$). These data are representative of the results from three independent experiments. (D) Whole-mount TUNEL assay. Albino embryos injected with the mRNA of Myt1 (50 pg) or β-Gal (50 pg) were fixed at stage 11 and processed for TUNEL staining. A positive TUNEL reaction is indicated by purple staining of the nuclei. (E) One-cell-stage *Xenopus* embryos were injected with the mRNA of Myt1 (70 pg) with/without that of DN-JNK1 (0.5 or 1.0 ng). The histogram represents the number of phenotypic changes. The asterisks indicate a significant decrease in dissociation compared to that for the control ($P < 0.05$). These data are representative of the results from three independent experiments. (F) One-cell-stage *Xenopus* embryos were injected with the mRNA of Myt1 (50 pg) with/without human JNK1 or human JNK2 (200 pg of each). The embryos shown were photographed at stage 12. (G and H) Histograms representing the number of phenotypic changes induced by Myt1 with/without JNK1 (G) or JNK2 (H). The asterisks indicate a significant increase (G) or decrease (H) in dissociation/death compared to that of the control ($P < 0.05$). These data are representative of the results from three independent experiments.

a tumor suppressor function of JNKs might be more prevalent than an oncogenic function (24). These results have clearly pointed out that distinctly different JNK functions might occur through the specific substrate choice or might be related to temporal aspects. However, specific substrates for JNK1, JNK2, or JNK3 are yet to be identified but very likely exist. To identify new specific substrates that might be associated with the distinct role of JNK1 and JNK2 in carcinogenesis, we screened interactions between JNK1, JNK2, or JNK3 and 60 kinases using the M2-H assay in vitro. The results presented here show that the membrane-associated inhibitory kinase Myt1 interacted with JNK1 and JNK3 but not JNK2. We also

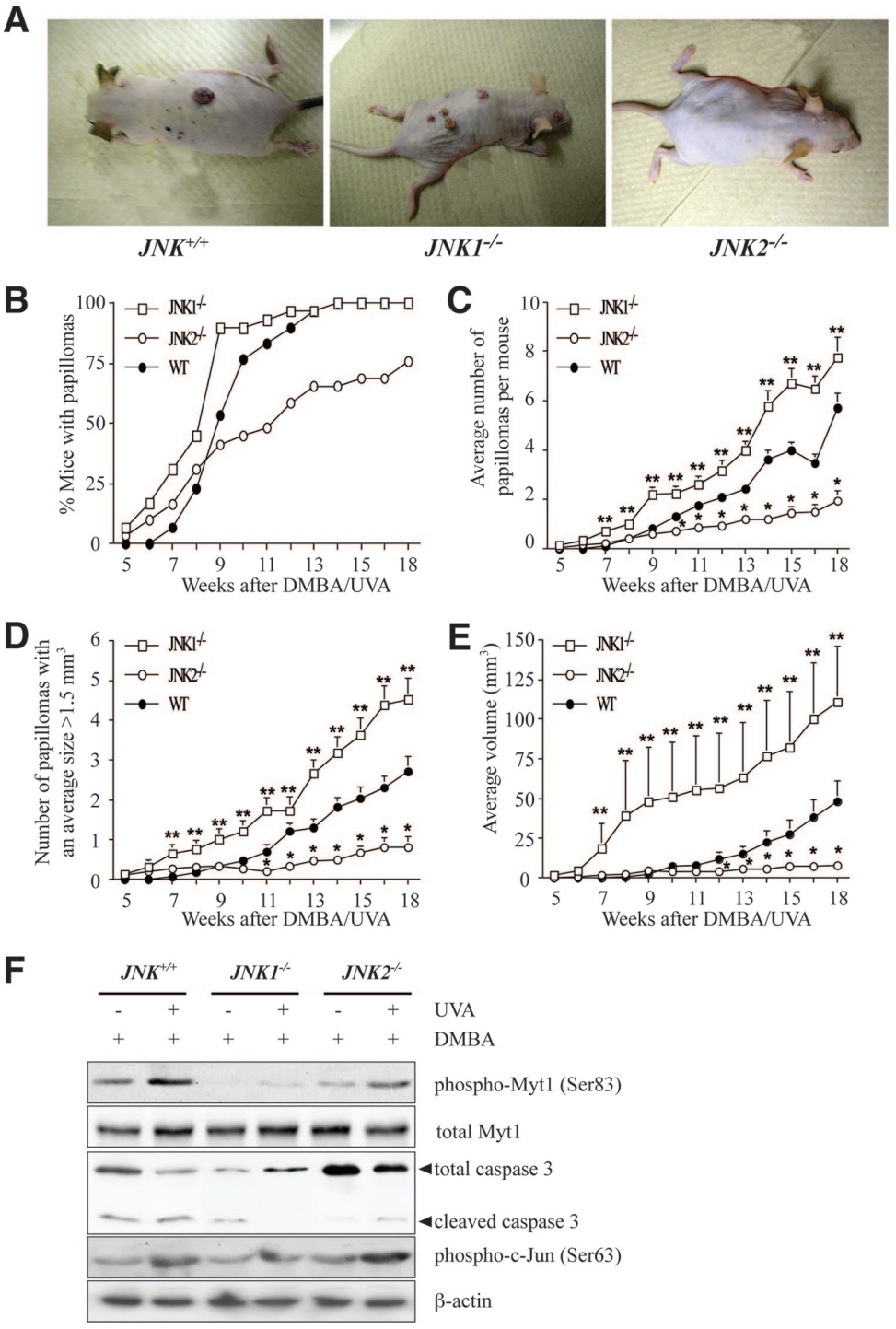

FIG. 6. The JNK1-mediated phosphorylation of Myt1 inhibits UVA-induced skin tumorigenesis in vivo. (A) External appearance of papillomas. Mice received one topical dose of DMBA (200 nmol in 250 μl acetone) and 2 weeks later were exposed to increasing doses of UVA five times a week (Monday through Friday) as follows: week 1, 4,200 J/m^2 or 3.5 min; week 2, 8,400 J/m^2 or 7 min; week 3, 16,800 J/m^2 or 14 min; week 4, 33,600 J/m^2 or 28 min; week 5, 67,200 J/m^2 or 56 min; week 6, 100,800 J/m^2 or 84 min; and weeks 7 to 18, 144,000 J/m^2 or 120 min. Mice were monitored and treated with UVA for 18 weeks after DMBA initiation treatment. (B) Fewer *JNK2*$^{-/-}$ mice than *JNK*$^{+/+}$ or *JNK1*$^{-/-}$ mice developed papillomas after exposure to UVA. (C) The average numbers of papillomas were significantly different among groups. A single asterisk indicates significantly ($P < 0.05$) fewer papillomas for *JNK2*$^{-/-}$ mice than for *JNK1*$^{-/-}$ or *JNK*$^{+/+}$ mice, and double asterisks indicate significantly ($P < 0.05$) more papillomas for *JNK1*$^{-/-}$ mice than for *JNK2*$^{-/-}$ or *JNK*$^{+/+}$ mice. Data are expressed as means ± standard errors (S.E.). (D) The average numbers of papillomas of >1.5 mm^3 were significantly different among groups. A single asterisk indicates significantly ($P < 0.05$) fewer papillomas of >1.5 mm^3 for *JNK2*$^{-/-}$ mice than for *JNK1*$^{-/-}$ or *JNK*$^{+/+}$ mice, and double asterisks indicate significantly ($P < 0.05$) more papillomas of >1.5 mm^3 for *JNK1*$^{-/-}$ mice than for *JNK2*$^{-/-}$ or *JNK*$^{+/+}$ mice. Data are expressed as means ± S.E. (E) Average papilloma volumes were significantly different among groups. A single asterisk indicates significantly ($P < 0.05$) smaller papillomas for *JNK2*$^{-/-}$ mice than for *JNK1*$^{-/-}$ or *JNK*$^{+/+}$ mice, and double asterisks indicate significantly ($P < 0.05$) larger papillomas for *JNK1*$^{-/-}$ mice than for *JNK2*$^{-/-}$ or *JNK*$^{+/+}$ mice. Data are expressed as means ± S.E. (F) Effect of UVA on the phosphorylation of Myt1 and the activity of caspase-3 in JNK WT and JNK-deficient mice. The dorsal skins from *JNK*$^{+/+}$, *JNK1*$^{-/-}$, and *JNK2*$^{-/-}$ mice were biopsied, and the total lysates were analyzed by immunoblotting using antibodies against the respective proteins. Reproducible results were obtained in three independent experiments, and representative blots are shown.

have shown here that both end-terminal domains of Myt1 are required for its interaction with a specific region of JNK1 or JNK3 (residues 1 to 205 or 1 to 240, respectively) and that JNK1 and JNK3 can phosphorylate Myt1 in vitro.

Myt1 is a dual-specificity kinase involved in cell cycle regulation (12) and is responsible for the inhibitory phosphorylation of the Cdk/cyclin complexes (25). In all eukaryotic cells, progression through the cell cycle is regulated by the sequential activation of the cyclin-dependent protein kinases (CDKs) (29, 32). The activation of the p34cdc2 (Cdc2) CDK is the universal event controlling the onset of mitosis. The ability of Cdc2 to induce the M phase is dependent on its association with a cyclin partner yet is also further regulated in positive and negative fashions by phosphorylation. Specifically, phosphorylation at Thr161 by the CDK-activating kinase is necessary for the activation of the CDK/cyclin complex, whereas the phosphorylation of Thr14 and Tyr15 by the Wee1 and Myt1 kinases maintains the complex in an inactive state (25, 30, 31). The dephosphorylation of Thr14 and Tyr15 upon the activation of the dual-specificity phosphatase Cdc25 coupled with the inactivation of the Thr14 and Tyr15 kinases results in the precipitate activation of cyclin B/Cdc2, which triggers the M phase (27, 36). In mitosis, the activity of Myt1 is decreased two- to fivefold, and Myt1 loses the ability to bind to cyclin B1 in mitotic extracts (25). Multiple kinases have been shown to phosphorylate Myt1, including Akt (33), p90RSK (35), Mos (37), Plk (19), and Cdc2/cyclin B (46). Although the role of Myt1 in the regulation of the cell cycle has been well characterized, little is known regarding the role of Myt1 in mediating cellular apoptosis and preventing UVA-induced skin carcinogenesis. Here, we demonstrated that UVA induced the association of JNK1 with Myt1 and that the UVA-induced phosphorylation of Myt1 activates cellular apoptosis and DNA fragmentation in the skin cancer cell line SK-MEL-28. In contrast, Myt1 knockdown results in resistance to UVA-induced apoptosis and DNA fragmentation in SK-MEL-28 cells. A number of lines of evidence have suggested a possible involvement of the mitosis-promoting protein kinase Cdc2 in the process of apoptotic cell death, and one recent study concluded that the inactivation of Cdc2 increases the level of apoptosis induced by DNA damage (34). Here, we showed that the UVA-induced phosphorylation of Myt1 in $JNK^{+/+}$ or $JNK2^{-/-}$ MEFs mediated the phosphorylation of Cdc2 (Tyr15), which inactivates Cdc2, whereas the phosphorylation of Cdc2 (Tyr15) was suppressed in $JNK1^{-/-}$ MEFs, suggesting that the JNK1 phosphorylation of Myt1 plays a key role in the inactivation of Cdc2 concomitant with apoptosis. The caspase family of aspartate-specific cysteine proteases has been shown to be central executors of apoptosis (5). Caspase-3 is the key player and is activated in a variety of cell types during apoptosis. It is responsible for the proteolytic cleavage of a set of proteins, such as the nuclear enzyme poly(ADP-ribose) polymerase (13). It was reported that the deregulation of Cdc2 kinase activity can trigger apoptotic machinery that leads to caspase-3 activation and apoptosis (16). In a recent report, the activation of the intrinsic mitochondrial apoptosis pathway by the $p14^{ARF}$ tumor suppressor, which is preceded by the downregulation of Cdc2 expression, was confirmed by cytochrome *c* release from mitochondria and the induction of caspase-9- and caspase-3/7-like activities (17). In line with this, we show that UVA-induced caspase-3 cleavage and apoptosis were markedly inhibited in Myt1 knockdown cells, which are the negative regulator of Cdc2. Also, the overexpression of DN-Myt1 suppressed UVA-induced caspase-3 activation, which may explain the mechanism of Myt1-induced apoptosis. Interestingly, UVA phosphorylated Myt1 in $JNK^{+/+}$ or $JNK2^{-/-}$ MEFs, whereas the phosphorylation of Myt1 induced by UVA was suppressed in $JNK1^{-/-}$ MEFs. Furthermore, the overexpression of Myt1 promotes cellular apoptosis during the early embryonic development of *Xenopus laevis*. In addition, the overexpression of JNK1 with Myt1 enhances apoptotic cell death in *Xenopus* embryos, whereas the overexpression of JNK2 suppresses the phenotype of Myt1-induced apoptotic cell death. Taken together, these data suggest that the JNK1-mediated phosphorylation of Myt1 triggers apoptosis when induced by UVA.

The balance between cell growth, differentiation, and apoptosis affects the net numbers of cells in the body, and the aberrant regulation of these processes can give rise to tumors (45). Dysregulated apoptosis contributes to many pathologies, including tumor promotion, autoimmune and immunodeficiency diseases, and neurodegenerative disorders (11, 51). The JNK pathway is activated by the exposure of cells to stress. However, the role of JNK in the stress response is not totally clear. Initial studies examining JNK's role in apoptosis were performed by investigating neuronal cell death in response to neurotrophic factor withdrawal (48). In this report, nerve growth factor withdrawal led to the sustained activation of JNKs, which caused the induction of apoptosis during neuronal development (48). The tumor suppressor p53 is another potential target of proapoptotic signaling by JNK, which phosphorylates murine p53 on Ser34 in vitro (28). Binding to JNK was reported to phosphorylate p53, inhibit ubiquitin-mediated degradation, and thus stabilize the p53 protein (14, 15). These data suggested that JNK might be important for controlling the level of p53 expression by regulating the half-life of p53. Our analysis demonstrates that the JNK2-null MEFs and mice exhibit significantly increased cleavage of caspase-3 after exposure to UVA concomitant with the phosphorylation of Myt1, whereas caspase-3 cleavage was attenuated in JNK1-null MEFs and mice. In addition, UVA dramatically induced DNA fragmentation in $JNK^{+/+}$ or $JNK2^{-/-}$ MEFs, whereas UVA-induced DNA fragmentation was suppressed in $JNK1^{-/-}$ MEFs. Furthermore, UVA-induced caspase-3 cleavage and DNA fragmentation were markedly inhibited in the Myt1 knockdown of SK-MEL-28 cells. In conclusion, we suggest that JNK1-mediated phosphorylation of Myt1 is required for the induction of apoptosis in skin cancer, supporting the idea that JNK1 and JNK2 can specifically function as tumor suppressors or as oncokinases, respectively.

Here, we examined the molecular mechanisms of UV-induced apoptosis that affect tumor development in skin. We also investigated how different JNK isoforms can lead to resistance to or promote carcinogenesis. Our findings indicate that JNK1 protein kinase contributes to cellular apoptosis in mouse fibroblasts or human skin melanoma cells, followed by the JNK1-mediated phosphorylation of Myt1. On the contrary, JNK2 protein kinase appears to primarily function as a positive regulator of carcinogenesis. This conclusion is fully consistent with the results of previous studies that JNK2 activity increased c-Jun expression and cellular proliferation (21). This under-

standing has critical implications for the molecular mechanism of JNK signaling and the use of this pathway as a target for therapeutic strategies for the treatment of skin cancer.

ACKNOWLEDGMENTS

This work was supported by The Hormel Foundation and grants from the National Institutes of Health (CA027502, R37CA081964, CA077646, CA111536, CA120388, and ES016548).

REFERENCES

1. **Bachelor, M. A., and G. T. Bowden.** 2004. UVA-mediated activation of signaling pathways involved in skin tumor promotion and progression. Semin. Cancer Biol. **14:**131–138.
2. **Bode, A. M., and Z. Dong.** 2007. The functional contrariety of JNK. Mol. Carcinog. **46:**591–598.
3. **Caffrey, D. R., L. A. O'Neill, and D. C. Shields.** 1999. The evolution of the MAP kinase pathways: coduplication of interacting proteins leads to new signaling cascades. J. Mol. Evol. **49:**567–582.
4. **Carter, A. D., and J. C. Sible.** 2003. Loss of XChk1 function triggers apoptosis after the midblastula transition in Xenopus laevis embryos. Mech. Dev. **120:**315–323.
5. **Chang, H. Y., and X. Yang.** 2000. Proteases for cell suicide: functions and regulation of caspases. Microbiol. Mol. Biol. Rev. **64:**821–846.
6. **Chen, F., Z. Zhang, S. S. Leonard, and X. Shi.** 2001. Contrasting roles of NF-kappaB and JNK in arsenite-induced p53-independent expression of GADD45alpha. Oncogene **20:**3585–3589.
7. **Choi, B. Y., H. S. Choi, K. Ko, Y. Y. Cho, F. Zhu, B. S. Kang, S. P. Ermakova, W. Y. Ma, A. M. Bode, and Z. Dong.** 2005. The tumor suppressor p16(INK4a) prevents cell transformation through inhibition of c-Jun phosphorylation and AP-1 activity. Nat. Struct. Mol. Biol. **12:**699–707.
8. **Davis, R. J.** 2000. Signal transduction by the JNK group of MAP kinases. Cell **103:**239–252.
9. **de Laat, A., J. C. van der Leun, and F. R. de Gruijl.** 1997. Carcinogenesis induced by UVA (365-nm) radiation: the dose-time dependence of tumor formation in hairless mice. Carcinogenesis **18:**1013–1020.
10. **Dong, Z., R. H. Xu, J. Kim, S. N. Zhan, W. Y. Ma, N. H. Colburn, and H. Kung.** 1996. AP-1/jun is required for early Xenopus development and mediates mesoderm induction by fibroblast growth factor but not by activin. J. Biol. Chem. **271:**9942–9946.
11. **Evan, G., and T. Littlewood.** 1998. A matter of life and cell death. Science **281:**1317–1322.
12. **Fattaey, A., and R. N. Booher.** 1997. Myt1: a Wee1-type kinase that phosphorylates Cdc2 on residue Thr14. Prog. Cell Cycle Res. **3:**233–240.
13. **Fernandes-Alnemri, T., G. Litwack, and E. S. Alnemri.** 1994. CPP32, a novel human apoptotic protein with homology to Caenorhabditis elegans cell death protein Ced-3 and mammalian interleukin-1 beta-converting enzyme. J. Biol. Chem. **269:**30761–30764.
14. **Fuchs, S. Y., V. Adler, T. Buschmann, Z. Yin, X. Wu, S. N. Jones, and Z. Ronai.** 1998. JNK targets p53 ubiquitination and degradation in nonstressed cells. Genes Dev. **12:**2658–2663.
15. **Fuchs, S. Y., V. Adler, M. R. Pincus, and Z. Ronai.** 1998. MEKK1/JNK signaling stabilizes and activates p53. Proc. Natl. Acad. Sci. USA **95:**10541–10546.
16. **Gu, L., H. Zheng, S. A. Murray, H. Ying, and Z. X. Jim Xiao.** 2003. Deregulation of Cdc2 kinase induces caspase-3 activation and apoptosis. Biochem. Biophys. Res. Commun. **302:**384–391.
17. **Hemmati, P. G., G. Normand, B. Gillissen, J. Wendt, B. Dorken, and P. T. Daniel.** 2008. Cooperative effect of p21Cip1/WAF-1 and 14-3-3sigma on cell cycle arrest and apoptosis induction by p14ARF. Oncogene **27:**6707–6719.
18. **Hensey, C., and J. Gautier.** 1997. A developmental timer that regulates apoptosis at the onset of gastrulation. Mech. Dev. **69:**183–195.
19. **Inoue, D., and N. Sagata.** 2005. The Polo-like kinase Plx1 interacts with and inhibits Myt1 after fertilization of Xenopus eggs. EMBO J. **24:**1057–1067.
20. **Ip, Y. T., and R. J. Davis.** 1998. Signal transduction by the c-Jun N-terminal kinase (JNK)—from inflammation to development. Curr. Opin. Cell Biol. **10:**205–219.
21. **Jaeschke, A., M. Karasarides, J. J. Ventura, A. Ehrhardt, C. Zhang, R. A. Flavell, K. M. Shokat, and R. J. Davis.** 2006. JNK2 is a positive regulator of the cJun transcription factor. Mol. Cell **23:**899–911.
22. **Johnson, R., B. Spiegelman, D. Hanahan, and R. Wisdom.** 1996. Cellular transformation and malignancy induced by ras require c-jun. Mol. Cell. Biol. **16:**4504–4511.
23. **Kelfkens, G., F. R. de Gruijl, and J. C. van der Leun.** 1991. Tumorigenesis by short-wave ultraviolet A: papillomas versus squamous cell carcinomas. Carcinogenesis **12:**1377–1382.
24. **Kennedy, N. J., H. K. Sluss, S. N. Jones, D. Bar-Sagi, R. A. Flavell, and R. J. Davis.** 2003. Suppression of Ras-stimulated transformation by the JNK signal transduction pathway. Genes Dev. **17:**629–637.
25. **Liu, F., C. Rothblum-Oviatt, C. E. Ryan, and H. Piwnica-Worms.** 1999. Overproduction of human Myt1 kinase induces a G_2 cell cycle delay by interfering with the intracellular trafficking of Cdc2-cyclin B1 complexes. Mol. Cell. Biol. **19:**5113–5123.
26. **Lu, C., F. Zhu, Y. Y. Cho, F. Tang, T. Zykova, W. Y. Ma, A. M. Bode, and Z. Dong.** 2006. Cell apoptosis: requirement of H2AX in DNA ladder formation, but not for the activation of caspase-3. Mol. Cell **23:**121–132.
27. **McGowan, C. H., and P. Russell.** 1995. Cell cycle regulation of human WEE1. EMBO J. **14:**2166–2175.
28. **Milne, D. M., L. E. Campbell, D. G. Campbell, and D. W. Meek.** 1995. p53 is phosphorylated in vitro and in vivo by an ultraviolet radiation-induced protein kinase characteristic of the c-Jun kinase, JNK1. J. Biol. Chem. **270:**5511–5518.
29. **Morgan, D. O.** 1997. Cyclin-dependent kinases: engines, clocks, and microprocessors. Annu. Rev. Cell Dev. Biol. **13:**261–291.
30. **Mueller, P. R., T. R. Coleman, and W. G. Dunphy.** 1995. Cell cycle regulation of a Xenopus Wee1-like kinase. Mol. Biol. Cell **6:**119–134.
31. **Mueller, P. R., T. R. Coleman, A. Kumagai, and W. G. Dunphy.** 1995. Myt1: a membrane-associated inhibitory kinase that phosphorylates Cdc2 on both threonine-14 and tyrosine-15. Science **270:**86–90.
32. **Norbury, C., J. Blow, and P. Nurse.** 1991. Regulatory phosphorylation of the p34cdc2 protein kinase in vertebrates. EMBO J. **10:**3321–3329.
33. **Okumura, E., T. Fukuhara, H. Yoshida, S. Hanada, R. Kozutsumi, M. Mori, K. Tachibana, and T. Kishimoto.** 2002. Akt inhibits Myt1 in the signalling pathway that leads to meiotic G2/M-phase transition. Nat. Cell Biol. **4:**111–116.
34. **Ongkeko, W., D. J. Ferguson, A. L. Harris, and C. Norbury.** 1995. Inactivation of Cdc2 increases the level of apoptosis induced by DNA damage. J. Cell Sci. **108:**2897–2904.
35. **Palmer, A., A. C. Gavin, and A. R. Nebreda.** 1998. A link between MAP kinase and p34(cdc2)/cyclin B during oocyte maturation: p90(rsk) phosphorylates and inactivates the p34(cdc2) inhibitory kinase Myt1. EMBO J. **17:**5037–5047.
36. **Parker, L. L., P. J. Sylvestre, M. J. Byrnes III, F. Liu, and H. Piwnica-Worms.** 1995. Identification of a 95-kDa WEE1-like tyrosine kinase in HeLa cells. Proc. Natl. Acad. Sci. USA **92:**9638–9642.
37. **Peter, M., J. C. Labbe, M. Doree, and E. Mandart.** 2002. A new role for Mos in Xenopus oocyte maturation: targeting Myt1 independently of MAPK. Development **129:**2129–2139.
38. **Pulverer, B. J., J. M. Kyriakis, J. Avruch, E. Nikolakaki, and J. R. Woodgett.** 1991. Phosphorylation of c-jun mediated by MAP kinases. Nature **353:**670–674.
39. **She, Q. B., N. Chen, A. M. Bode, R. A. Flavell, and Z. Dong.** 2002. Deficiency of c-Jun-NH(2)-terminal kinase-1 in mice enhances skin tumor development by 12-O-tetradecanoylphorbol-13-acetate. Cancer Res. **62:**1343–1348.
40. **Sible, J. C., J. A. Anderson, A. L. Lewellyn, and J. L. Maller.** 1997. Zygotic transcription is required to block a maternal program of apoptosis in Xenopus embryos. Dev. Biol. **189:**335–346.
41. **Smeal, T., B. Binetruy, D. A. Mercola, M. Birrer, and M. Karin.** 1991. Oncogenic and transcriptional cooperation with Ha-Ras requires phosphorylation of c-Jun on serines 63 and 73. Nature **354:**494–496.
42. **Stack, J. H., and J. W. Newport.** 1997. Developmentally regulated activation of apoptosis early in Xenopus gastrulation results in cyclin A degradation during interphase of the cell cycle. Development **124:**3185–3195.
43. **Sterenborg, H. J., and J. C. van der Leun.** 1990. Tumorigenesis by a long wavelength UV-A source. Photochem. Photobiol. **51:**325–330.
44. **Tournier, C., P. Hess, D. D. Yang, J. Xu, T. K. Turner, A. Nimnual, D. Bar-Sagi, S. N. Jones, R. A. Flavell, and R. J. Davis.** 2000. Requirement of JNK for stress-induced activation of the cytochrome c-mediated death pathway. Science **288:**870–874.
45. **Vaux, D. L., and S. J. Korsmeyer.** 1999. Cell death in development. Cell **96:**245–254.
46. **Wells, N. J., N. Watanabe, T. Tokusumi, W. Jiang, M. A. Verdecia, and T. Hunter.** 1999. The C-terminal domain of the Cdc2 inhibitory kinase Myt1 interacts with Cdc2 complexes and is required for inhibition of G(2)/M progression. J. Cell Sci. **112:**3361–3371.
47. **Weston, C. R., and R. J. Davis.** 2002. The JNK signal transduction pathway. Curr. Opin. Genet. Dev. **12:**14–21.
48. **Xia, Z., M. Dickens, J. Raingeaud, R. J. Davis, and M. E. Greenberg.** 1995. Opposing effects of ERK and JNK-p38 MAP kinases on apoptosis. Science **270:**1326–1331.
49. **Xu, R. H., Z. Dong, M. Maeno, J. Kim, A. Suzuki, N. Ueno, D. Sredni, N. H. Colburn, and H. F. Kung.** 1996. Involvement of Ras/Raf/AP-1 in BMP-4 signaling during Xenopus embryonic development. Proc. Natl. Acad. Sci. USA **93:**834–838.
50. **Yang, D. D., D. Conze, A. J. Whitmarsh, T. Barrett, R. J. Davis, M. Rincon, and R. A. Flavell.** 1998. Differentiation of CD4+ T cells to Th1 cells requires MAP kinase JNK2. Immunity **9:**575–585.
51. **Yuan, J., and B. A. Yankner.** 1999. Caspase activity sows the seeds of neuronal death. Nat. Cell Biol. **1:**E44–E45.